Hindawi
International Journal of Antennas and Propagation
Volume 2022, Article ID 7847015, 10 pages
https://doi.org/10.1155/2022/7847015

Research Article

Compact Quadband Bandstop Filter Based on Concentric Split Ring Resonators with Perturbation for Multifunctional Wireless Systems

Pierre Moukala Mpele [1,2]

[1]*Faculty of Sciences and Techniques, Electrical and Electronics Engineering Laboratory, Marien Ngouabi University, B.P 69, Brazzaville, Congo*
[2]*Department of Electrical Engineering, Pan African University Institute for Basic Sciences Technology and Innovation, Nairobi, Kenya*

Correspondence should be addressed to Pierre Moukala Mpele; pm.mpele@gmail.com

Received 6 January 2022; Revised 16 March 2022; Accepted 21 March 2022; Published 20 May 2022

Academic Editor: Chien-Jen Wang

Bandstop filters play an essential role in many radio frequency (RF) and microwave communication systems to block undesired signals or reject spurious harmonics. This paper presents the design and experiment of a compact quadband bandstop filter centered at 1.2/1.97/2.96/4.78 GHz with a passband insertion loss ranging from 1.07 to 2.9 dB. The overall volumetric size of the proposed filter is $0.197\lambda_g \times 0.197\lambda_g \times 0.01\lambda_g$, where λ_g is the guided wavelength at 1.2 GHz. The desired performance is achieved by introducing two diamond-shaped concentric split ring resonators (DSCSRRs) intercoupled and defected ground structure. The metamaterial properties of the DSCSRR have been verified by extracting and analyzing its effective permittivity and permeability. This research shows that DSCSRRs can generate multiband characteristics and yield high selectivity with good band-to-band isolation by generating transmission zeros between passbands. The filter is designed, optimized, and analyzed using High-Frequency Structural Simulator (HFSS). A good agreement is observed between simulated and experimental results. The measured results demonstrate that the proposed quadband banstop filter exhibits a minimum stopband rejection of 11.22 dB and fractional bandwidth greater than 4.51%, which makes it suitable for front-end transceiver components or multifunctional wireless systems to suppress unwanted signals at four separate frequency bands.

1. Introduction

The suppression of unwanted frequency ranges and noise avoidance are essential issues in microwave and wireless communication systems. Band-stop filters perform this particular role owing to their band rejection ability. Besides, with the diversity of wireless applications, the demand for multifrequency filtering elements has increased. However, unlike multiband bandpass filters [1–7], multiband bandstop filters have not been as widely explored [8]. Also, the majority of multiband banstop filter design developed in the last decade were mostly concentrated on dual band and triband filtering responses [9–11]. In the literature, Split Ring Resonators (SRRs) are widely used in metamaterial cell configurations where the concept of single- and double-negative media can be exploited to reconfigure bandstop filters to bandpass filters (and vice versa) in both technologies [12]. Moreover, metamaterials though SRRs help in achieving the miniaturization of a filter structure with low insertion loss, and high out off-band rejection [13].

Unlike other microstrip passive components, quadband bandstop filter designs are relatively less in the scientific literature, to the best of the author's knowledge. In [14], a compact quadband bandstop filter using square spiral resonators based on folded stepped impedance resonators, while dual-plane defected structures and open-loop resonators have been employed to develop a quadband bandstop filter in [15]. Another technique has been suggested for

quadband filtering response based on coupled-line and shorted stub-loaded half-wavelength microstrip resonator. The quad-section stepped impedance open stub was proposed in [16], whereas the dual-mode open-loop resonators having thin-film capacitors in [17]. In addition to the aforementioned work, multiple-mode resonator have also been explored for quadband filtering characteristic [18].

This paper introduces and discusses a new quadband bandstop filter with diamond-shaped concentric split ring resonators (DSCSRRs). The DSCSRRs exhibit simultaneously single negative and double-negative behaviors in some particular frequency ranges. Those properties are helpful in microwave engineering. The proposed filter is compact and generates four transmission zeros which improve the selectivity and yield a high band to band isolation. Finally, the proposed quadband bandstop filter is analyzed, fabricated, and measured to validate its performance. A good agreement is found between simulated and measured results. The proposed filter has good performance in stopbands as well as passbands. It is cost-effective and easy to manufacture, making it an outstanding candidate for use in multifunctional wireless communication systems.

2. Filter Design

The main focus of this research is to construct a bandstop filter to reduce interferences from received signal. The proposed quadband bandstop filter is based on diamond-shaped concentric split ring resonators (DSCSRRs), designed and fabricated using a 1.524 mm thick FR-4 substrate with a permittivity of 4.4 and a loss tangent of 0.02. The design geometry configuration is presented in Figure 1 below.

In addition to using the DSCSRRs, a diamond-shaped slot whose configuration is depicted in Figure 1(b) is inserted in the ground plane, yielding the proposed filter configuration. In Figure 2, the width of each open ring is the same, with the distance separating two consecutive open-loops. The optimized design parameters of the proposed filter are provided in Table 1.

2.1. Filter Design Procedure. This section presents the main steps that have been used to design the hybrid quadband bandstop investigated in this paper.

The design starts with a simple diamond-shaped fed by using two microstrip transmission lines (Figure 2(a)). The corresponding frequency response presented in Figure 3(a) shows bandstop filter characteristics with a 3 dB cutoff frequency at 1.17 GHz. The filter has poor sharpness and stopband rejection while achieving an ultrawideband operation with a 6-dB fractional bandwidth of 105.65% though. Also, two passbands are observed at 5.16 GHz and 6.92 GHz with a return loss of 14.3 dB and 13.73 dB, respectively. The passband insertion loss is 2.09 dB and 2.6 dB for the first and the second passband. No transmission zero is observed at this stage. This implies that the filter exhibits poor selectivity.

In the second step (Figure 2(b)), the interior metallization of the patch is removed. The frequency response displayed in Figure 3(b) illustrates a dual-band lowpass-bandpass behavior similar to the design proposed in [19]. But, in this case, the band-to-band isolation is relatively poor, with a maximum stopband rejection of 4.1 dB. The 3 dB cutoff frequency of the lowpass filter is fount at 4.75 GHz, and the bandpass resonant frequency of the bandpass filter is 6.42 GHz with 1.23 dB insertion loss. Also, the frequency response illustrates two transmission poles (reflection zeros) located at 1.2 GHz and 4 GHz in the lowpass filter. This kind of filter can be used in some applications such as mixers and hybrid fiber-coaxial supported systems [20].

The third step of the design procedure is shown in Figure 2(c). As it can be seen, a split is etched on the diamond-shaped loop created in Step 2 above. This leads to an ultrawide stopband filter with a 3 dB fractional bandwidth of 86.62%, as illustrated by the frequency response shown in Figure 3(c). Besides, a transmission zero (TZ) is observed at 2.92 GHz with 35.04 dB stopband rejection, improving filter selectivity. Two transmission poles are also displayed at 5.1 GHz and 6.5 GHz with passband insertion loss of 1.72 dB and 1.35 dB. It is important to note that up to this stage, the filter does not exhibit a multiband bandstop characteristic as from Figures 3(a)–3(c).

To address this, a diamond-shaped concentric split ring resonators (DSCSRRs) unit cell is designed and inserted to the design configuration (Figure 2(d)) along with the 45°-rotated square slot in the ground plane. The multiband behavior is achieved. From Figure 3(d), a quadband-bandstop behavior is observed. Four transmission zeros are obtained at 1.31 GHz, 1.92 GHz, 2.75 GHz, and 4.22 GHz with 13.82 dB, 11.02 dB, 28.82 dB, and 22.83 dB stopband rejection, respectively. The corresponding return loss at these stopbands is 2.28 dB, 3.1 dB, 0.58 dB, and 0.87 dB. This illustrates a good stopband rejection characteristic for the proposed quadband bandstop filter.

Moreover, in the passbands, the insertion loss is 0.81 dB, 1.59 dB, and 2.9 dB at the respective resonant frequencies, which are 1.41 GHz, 2.01 GHz, and 3.72 GHz. The corresponding return loss is 23.86 dB, 17 dB, and 11.81 dB. These performance parameters are further validated by manufacturing the filter prototype and taking measurements.

The proposed quadband bandstop filter can be modeled by an equivalent circuit made of passive lumped elements (inductor and capacitor in parallel grouping) based on the theory of the stopband filter described in [21] where the following formulas are employed to calculate the elements,

$$C = \frac{1}{2\pi Z\left(f_u - f_l\right)}, \qquad L = \frac{1}{4\pi^2 f_0^2 C}. \tag{1}$$

f_u and f_l are upper and lower cutoff frequencies at −10 dB, f_0 is the resonant frequency, and Z denotes the input impedance of filter and can be obtained from the simulated results.

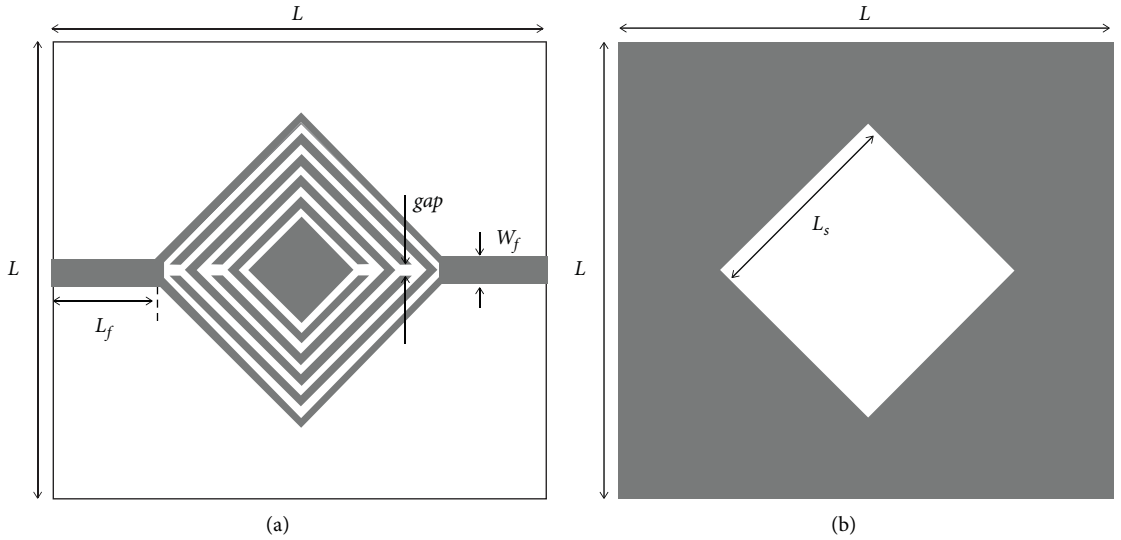

Figure 1: Proposed filter design configuration: (a) top view, (b) bottom view.

Table 1: Optimized design parameters of the proposed filter.

Parameter	Value (mm)
L	30
L_f	5.4755
L_S	11.5
L_p	14
L_u	12.5
W_f	0.75
gap	0.1
s	0.375

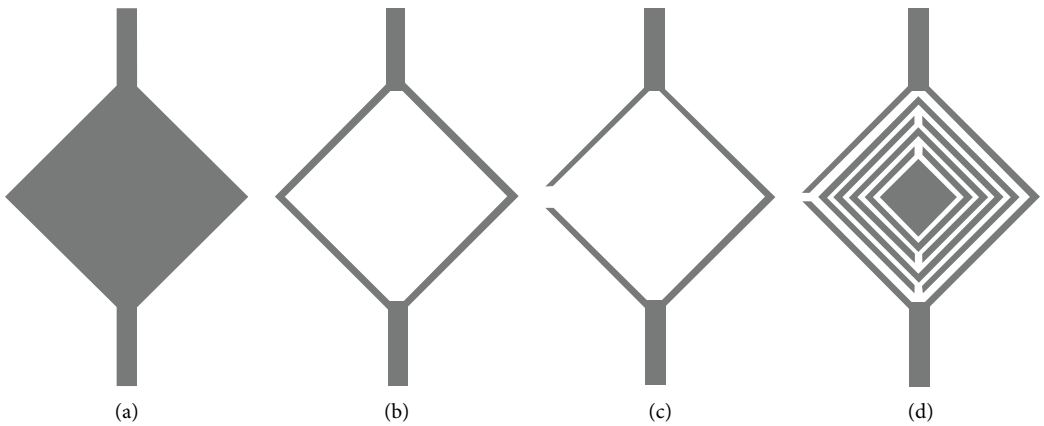

Figure 2: Design procedure of the proposed filter: (a) Step 1, (b) Step 2, (c) Step 3, and (d) Step 4.

Figure 4 illustrates the equivalent resonant circuit model of the proposed quadband bandstop filter in which each stopband is modeled as a parallel LC resonant circuit.

2.2. Diamond-Shaped Concentric Split Ring Resonators (DSCSRRs). In this research, DSCSRRs are studied, and their fundamental properties are investigated. The coupling between the resonators is controlled by the line width "s" of the line separating two consecutive diamond-shaped loops, as shown in Figure 5. Increasing the line width "*s*" between the resonators will decrease coupling and consequently decrease the stopband bandwidth. A split-ring resonator (SRR) is commonly involved as an elementary cell for producing a magnetic response [22]. The proposed DSCSRRs unit cell shown in Figure 5 is designed on top of a

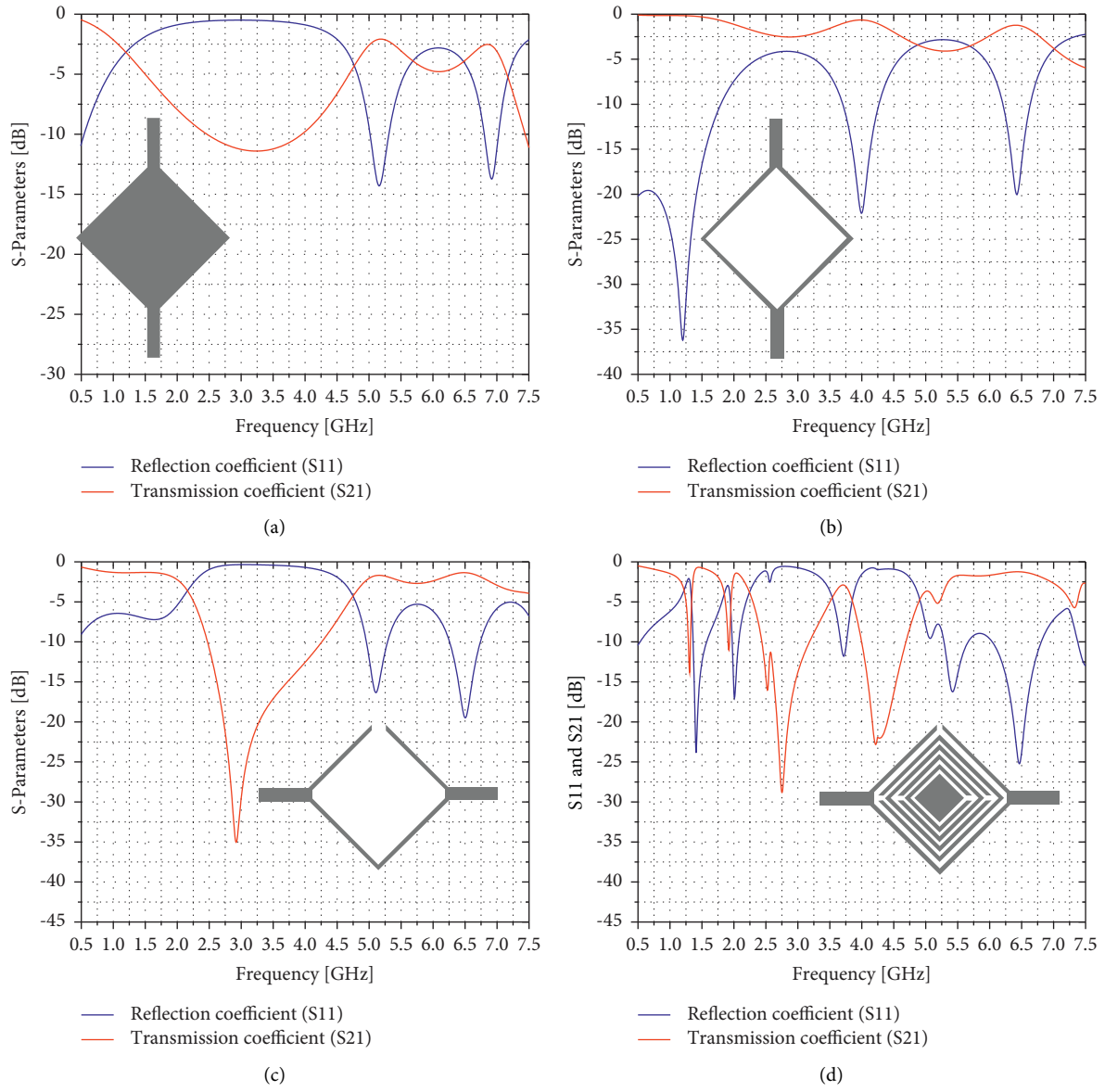

Figure 3: Design process of the proposed hybrid quadband lowpass-passband filter: (a) Step 1, (b) Step 2, (c) Step 3, and (d) Step 4.

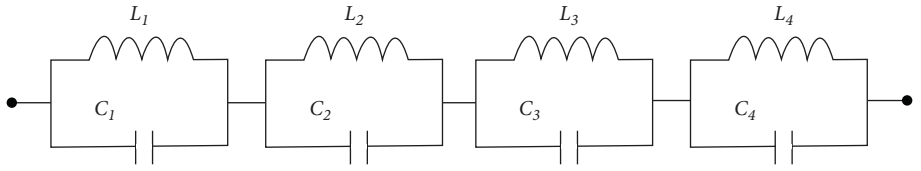

Figure 4: Equivalent LC circuit model of the designed filter.

$18 \times 18 \times 1.524\,\text{mm}^3$ FR-4 substrate and simulated using HFSS where a 1.5 mm width microstrip line is inserted to respond electrically to electromagnetic fields. The material's effective parameters are retrieved with a MATLAB computer code provided in [23].

Figure 5(b) presents the simulation setup for the proposed unit cell where the perfect electric and perfect magnetic conductor boundaries are employed along with wave ports to extract its main parameters. The Perfect Electric and Perfect Magnetic boundaries are applied to the pairs (1, 3)

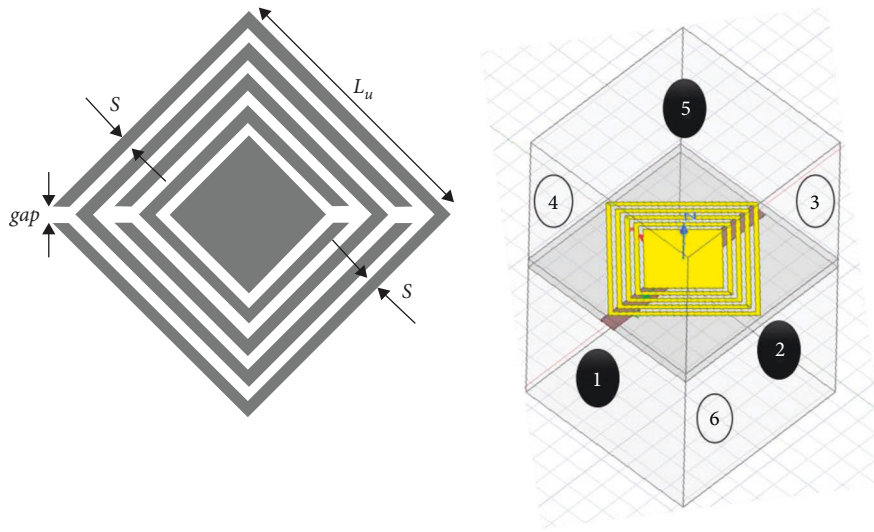

(a) (b)

Figure 5: (a) DSCSSRs unit cell configuration, (b) Unit cell simulation setup in HFSS.

and (2, 4) as boundary conditions. The wave port excitations are employed on the faces labeled "5" and "6."

From the metamaterial parameters retrieval techniques described in [23–25], effective permittivity and permeability are related to the simulated reflection (S_{11}) and transmission (S_{21}) coefficients by following equations,

$$n = \frac{1}{k_0 d}\cos^{-1}\left[\frac{1}{2S_{21}}\left(1 - S_{11}^2 + S_{21}^2\right)\right],$$
$$z = \pm\sqrt{\frac{(1+S_{11})^2 - S_{21}^2}{(1-S_{11})^2 - S_{21}^2}}. \quad (2)$$

n denotes the refractive index, k_0, the free space wavenumber, z, the wave impedance of the slab, ε the effective permittivity, μ, the effective permeability of the material, and d, the cell dimension.

The simulation is performed using HFSS, which is a 3D full wave simulator based on Finite Element method (FEM). The scattering parameters of the proposed unit cell are presented in Figure 6 below. It can be observed that the transmission coefficient achieves its lowest values at around 0.6 GHz and 5.26 GHz, whereas the resonance and filtering characteristics are seen from 2.25 GHz and above.

To further characterize the proposed DSCSRR unit cell, the real parts of the effective permittivity and permeability are extracted and presented in Figure 7. It can be observed that the DSCSRRs exhibit either a single negative (SNG) or double-negative (DNG) behavior in the frequency bands of interest, which are the most helpful metamaterial properties.

Contains Table 2 all the frequency responses for the proposed metamaterial unit cell. The extracted real permittivity and permeability are provided with their respective signs in the given frequency bands.

It can be observed that in the frequency regions 0.59–0.9 GHz, 4.38–4.81 GHz, 5.61–5.67 GHz, and 6.08–7.24 GHz, the proposed DSCSRR unit cell achieves positive real permittivity and permeability. The substrate provides a normal behavior of a standard insulator. This property does not add value in perturbating the current distribution or the electric field.

In the frequency ranges 1.85–2 GHz, 3.12–3.86 GHz, 5.67–6.08 GHz, and 7.24–7.5 GHz, the proposed unit cell performs a double-negative behavior, which affects allow waves to propagate in the opposite direction (backward waves). This behavior is commonly exploited for bandwidth in many applications, such as bandwidth improvement and miniaturization in microwave engineering. Lastly, the single negative behavior is observed from the regions 0.5–0.59 GHz, 0.9–1.85 GHz, 2–3.12 GHz, 3.86–4.38 GHz, 4.81–5.10 GHz, and 5.27–5.61 GHz. This filtering property slows down or blocks the wave's propagation, leading to a filtering behavior. This feature is commonly used for mutual coupling reduction in MIMO antenna systems and bandstop filters.

2.3. Realization of the Proposed Filter. Figure 8 displays a photograph of the filter prototype fabricated on a double-sided FR4 substrate using the high precision LPKF ProtoMat S103. The copper cladding top and bottom is 35 μm. The footprint of the proposed quadband filter is $30 \times 30\ \text{mm}^2 (0.197\lambda_g \times 0.197\lambda_g)$.

3. Results and Discussion

All the measurements were performed using R&S ZVA50 VNA. The proposed quadband filter's simulated and measured reflection coefficient is presented in Figure 9(a), whereas Figure 9(b) illustrates the transmission coefficient. A good agreement is achieved between simulated and measured results, which validates the proposed design

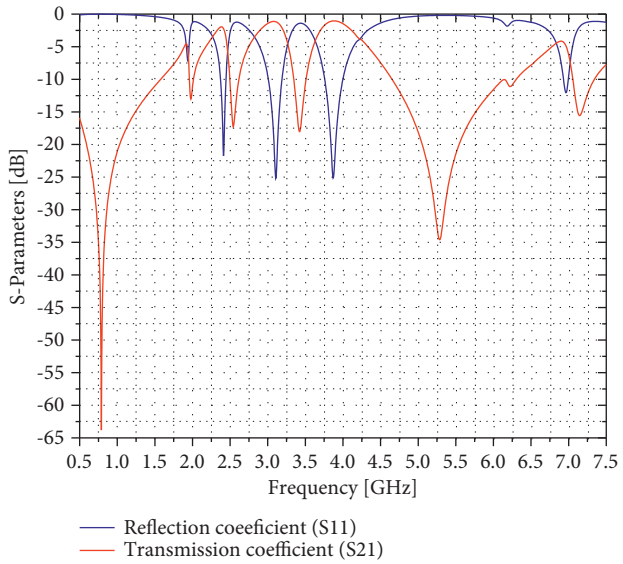

Figure 6: Scattering parameters of the DSCSRR.

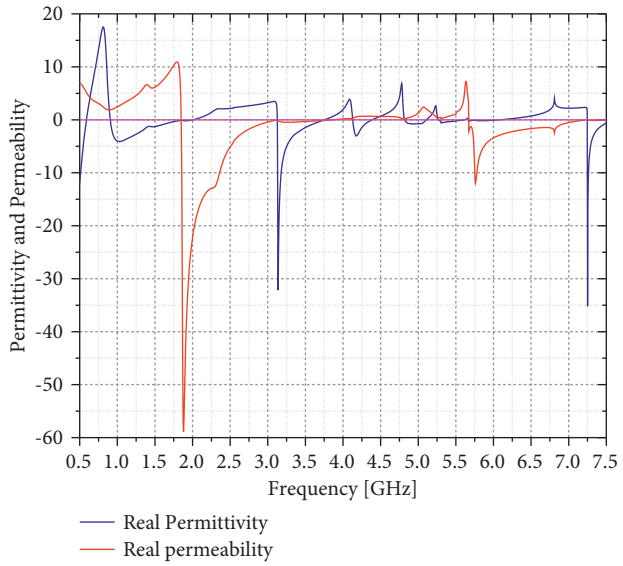

Figure 7: Retrieved real effective permittivity and permeability of the DSCSSRs.

Table 2: Extracted real permittivity and permeability values.

Frequency range	Real permittivity	Real permeability
0.5–0.59 GHz	Negative	Positive
0.59–0.9 GHz	Positive	Positive
0.9–1.85 GHz	Negative	Positive
1.85–2 GHz	Negative	Negative
2–3.12 GHz	Positive	Negative
3.12–3.76 GHz	Negative	Negative
3.76–3.86 GHz	Negative	Negative
3.86–4.13 GHz	Negative	Positive
4.13–4.38 GHz	Negative	Positive
4.38–4.81 GHz	Positive	Positive
4.81–5.10 GHz	Negative	Positive
5.10–5.27 GHz	Positive	Positive
5.27–5.61 GHz	Negative	Positive
5.61–5.67 GHz	Positive	Positive
5.67–6.08 GHz	Negative	Negative
6.08–7.24 GHz	Positive	Negative
7.24–7.5 GHz	Negative	Negative

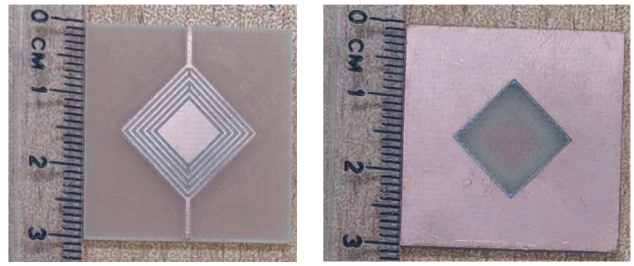

(a) (b)

Figure 8: Photograph of the fabricated prototype: (a) top view; (b) bottom view.

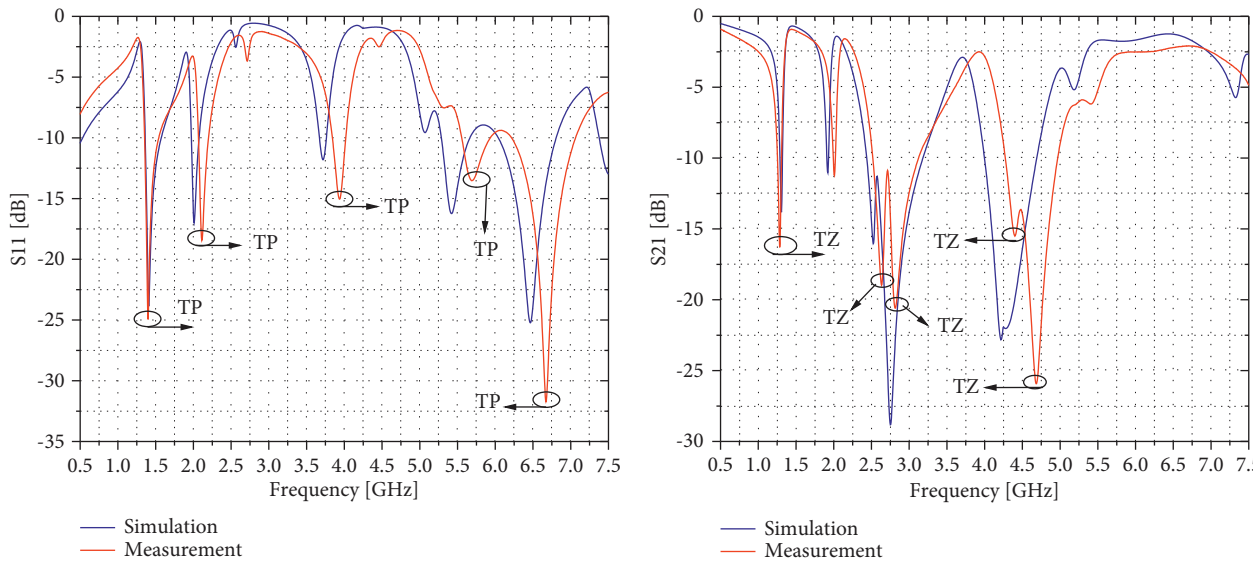

(a) (b)

Figure 9: Simulated and measured reflection and transmission coefficients of the proposed quadband filter: (a) reflection coefficient; (b) transmission coefficient.

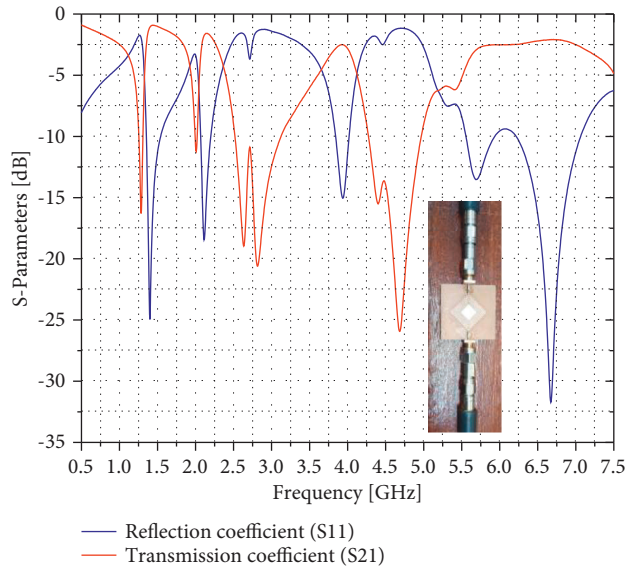

Figure 10: Measured reflection and transmission coefficient of the proposed quadband filter.

Table 3: Comparison between this work and other reported multiband bandstop filters.

Ref.	Stopbands	Center frequencies of stopbands (GHz)	Fractional bandwidth (%)	Size ($\lambda_g \times \lambda_g$)
[16]	4	1.24/3.2/6/8	40/30/25/26	0.139×0.171
[26]	4	1.16/1.58/1.94/2.37	5.2/6.9/2.9/1.3	0.26×0.25
[9]	3	1.8/2.4/3	20/12/22	0.44×0.44
[27]	3	3.8/6.7/9.5	19.2/6.7/3.3	0.682×0.325
[28]	2	1.4/2.57	12.7/10.11	0.650×0.380
[29]	3	2.24/4.8/6.52	79/26/13	0.090×0.310
[30]	2	3.35/5.75	6/1.7	0.270×0.270
This work	4	1.2/1.97/2.96/4.78	8.7/4.51/36.69/23.32	0.197×0.197

methodology and practically demonstrates the proposed configuration's effectiveness and advantages. Some of the slight discrepancies observed between simulated and measured results may be due to the soldering, reflections from the connectors, the finite substrate, or the manufacturing machine's precision.

3.1. Reflection Coefficient (S_{11}). The measured results presented in Figure 9(a) show return loss of 24.94 dB, 18.44 dB, 15.04 dB, 13.52 dB, and 31.64 dB at 1.4 GHz, 2.11 GHz, 3.93 GHz, 5.69 GHz, and 6.67 GHz, respectively. Five transmission poles (TP) are observed in Figure 10(a) whose the corresponding passband insertion loss is 1.07 dB, 1.76 dB, and 2.5 dB, 2.92 dB, and 2.08 dB. Besides, the -6 dB bandwidth is about 490 MHz (1.33–1.82 GHz), 260 MHz (2.04–2.3 GHz), and 360 MHz (3.73–4.09 GHz). This demonstrates that the proposed quadband bandstop filter can be used in several modern wireless applications such as GPS1200 (1227–1575 MHz), WMTS (1395–1400 MHz, 1427–1432 MHz), UMTS band I (1920–2170 MHz), 5G bands n77 (3.3–4.2 GHz), n78 (3.3–3.8 GHz), and a part of UWB range (3.1–5 GHz).

3.2. Transmission Coefficient (S_{21}). From both simulation and measurement transmission coefficient results displayed in Figure 9(b), the proposed filter configuration achieves four bandstops. The transmission coefficient analysis reveals stopbands centered (geometric mean) at 1.2 GHz, 1.97 GHz, 2.96 GHz, and 4.78 GHz, with a -6 dB fractional rejection bandwidth of 8.7%, 4.51%, 36.69%, and 23.32%. Moreover, the filter achieves six transmission zeros (TZ), which improves the selectivity with stopband rejection of 16.30 dB, 11.22 dB, 18.97 dB, 20.6 dB, 15.51 dB, and 25.92 dB, at 1.28 GHz, 2.01 GHz, 2.63 GHz, 2.81 GHz, 4.4 GHz, and 4.68 GHz, respectively. The return loss at the aforementioned stopband frequencies is about 1.92 dB, 3.58 dB, 1.59 dB, 1.39 dB, 2.02 dB, and 1.16 dB, which illustrates good bandstop performance for the proposed compact quadband filter.

It can be used for suppressing several unwanted modern wireless application signals, including LTE2300/2500, 5G band n40/n41/n77/n78, WiMAX3500, ISM/Bluetooth/Wi-Fi, GSM1800, C-band, and GPS1200 signals.

The measured results are summarized in Figure 10 above. It can be noticed that as the center frequency increases, the insertion loss increases for the passbands. The proposed bandstop filter achieves a −6 dB fractional bandwidth of 31.49%, 12%, and 9.22% for the first, the second, and the third passband bandpass span frequencies.

Transmission zeros separate the four passbands at 1.28 GHz, 2.01 GHz, 2.81 GHz, and 4.68 GHz giving 16.30 dB, 11.22 dB, 20.92 dB, and 15.51 dB stopband rejection, respectively. This results in high band-to-band isolation. The return loss in the passband between the stopbands is better than 15 dB, and the measured passband insertion loss is less than 2.5 dB. Finally, this proposed filter design can be suitably employed for RF/microwave modern and high-speed communications systems, owing to these encouraging results.

Table 3 gives a performance comparison with some reported multiple-band BSFs which shows that the proposed quadband bandstop filter in this work has compact size, wide fractional bandwidths, and good selectivity, in addition to the high band-to-band isolation around the rejection bands.

4. Conclusion

In this paper, a quadband bandstop filter loaded with DSCSRRs and a slot in the ground plane has been designed, fabricated, and tested. The filter does not have any additional matching network, which is advantageous in reducing its physical size. With a physical footprint of $30 \times 30\ mm^2$, the proposed device achieves a maximum passband insertion loss of about 2.5 dB and a return loss greater than 11 dB across all the frequency band of interest. Furthermore, it performs a minimum −6 dB passband bandwidth of 260 MHz, whereas the stopband fractional bandwidth greater than 4.5%. The merits of compact size, acceptable insertion loss, good return loss, high passband selectivity and band-to-band isolation make the proposed quadband stopband filter attractive in modern communication and sensor applications.

Data Availability

The data used to support the findings of this study are included within the article.

Conflicts of Interest

The author declares that there is no conflicts of interest regarding the publication of this paper.

References

[1] R. Gomez-Garcia, R. Loeches-Sanchez, D. Psychogiou, and D. Peroulis, "Multi-stub-loaded differential-mode planar multiband bandpass filters," *IEEE Transactions on Circuits and Systems II: Express Briefs*, vol. 65, no. 3, pp. 271–275, 2018.

[2] Y. Wu, E. Fourn, P. Besnier, and C. Quendo, "Direct synthesis of multiband bandpass filters with generalized frequency transformation methods," *IEEE Transactions on Microwave Theory and Techniques*, vol. 69, no. 8, pp. 3820–3831, 2021.

[3] K. Zhou, C. X. Zhou, H. W. Xie, and W. Wu, "Synthesis design of SIW multiband bandpass filters based on dual-mode resonances and split-type dual- and triple-band responses," *IEEE Transactions on Microwave Theory and Techniques*, vol. 67, no. 1, pp. 151–161, 2019.

[4] A. Basit and M. I. Khattak, "Designing modern compact microstrip planar quadband bandpass filter for hand held wireless applications," *Frequenz*, vol. 74, no. 5-6, pp. 219–227, 2020.

[5] J. Zhou, L. Wang, Z. Wang, S. Zhang, and M. He, "A compact quad-band bandpass filter with mixed electric and magnetic coupling," *International Journal of Microwave and Wireless Technologies*, vol. 11, no. 5-6, pp. 517–522, 2019.

[6] A. Sami, M. U. Rahman, and S. Bashir, "Design of compact tri and quad band band-pass filters using stub loaded resonators for wireless applications," *SN Applied Sciences*, vol. 1, pp. 1–9, 2019.

[7] L. Chen, X. Y. Li, and F. Wei, "A compact quad-band bandpass filter based on defected microstrip structure," *Frequenz*, vol. 71, pp. 311–316, 2017.

[8] N. Janković, V. Crnojević-Bengin, P. Meyer, and J.-S. Hong, "Design methods of multi-band filters," in *Advances in Multi-Band Microstrip Filters*, V. Crnojevic-Bengin, Ed., pp. 5–66, Cambridge University Press, Cambridge, UK, 2015.

[9] R. Ganesan and R. Sankararajan, "Design of a miniaturized tri-band bandstop filter using spur microstrip lines and via-hole grounding," *Circuit World*, vol. 46, no. 4, pp. 347–354, 2020.

[10] A. Batmanov, E. Burte, R. Mikuta, A. Boutejdar, A. Omar, and A. Khaidurova, "Design of coplanar bandstop filter based on open-loop-ring resonator and DGS for WLAN and UWB applications," in *Proceedings of the 2012 42nd European Microwave Conference*, pp. 1123–1126, IEEE, Amsterdam, The Netherlands, November 2012.

[11] C.-H. Wu, C.-C. Tang, and C.-W. Tang, "Design of the microstrip bandstop filter with high insertion loss," *IEEE Transactions on Components, Packaging, and Manufacturing Technology*, vol. 9, no. 1, pp. 122–128, 2019.

[12] A. K. Horestani, N. Varmazyar, F. Sadeghikia, M. T. Noghani, Z. Shaterian, and F. Martin, "On the applications of S-shaped split ring resonators (S-SRR) in sensors, filters, and antennas," in *Proceedings of the 2019 21st International Conference on Electromagnetics in Advanced Applications, ICEAA*, vol. 2019, pp. 485–488, Granada, Spaina, September 2019.

[13] Z. Troudi, J. Machac, and L. Osman, "Miniaturised planar band-pass filter based on interdigital Arm SRR," *IET Microwaves, Antennas & Propagation*, vol. 13, no. 12, pp. 2081–2086, 2019.

[14] P. Wang, H. Yang, Z. Yu, X. Huang, and Y. Jin, "A compact quad-band bandstop filter using square spiral resonators based on folded stepped impedance resonator," in *Proceedings of the 2016 11th International Symposium on Antennas, Propagation and EM Theory (ISAPE)*, pp. 766–768, IEEE, Guilin, China, October 2016.

[15] H. Ning, J. Wang, Q. Xiong, H. Liu, and L. Mao, "A compact quad-band bandstop filter using dual-plane defected structures and open-loop resonators," *IEICE Electronics Express*, vol. 9, no. 21, pp. 1630–1636, 2012.

[16] R. Banupriya, B. Purushothaman, and R. Shankaranarayanan, "Quad-band bandstop filter using quad-section stepped impedance open stub resonator," in *Proceedings of the 2016 International Conference on Communication and Signal Processing (ICCSP)*, pp. 0205–0207, IEEE, Melmaruvathur, India, April 2016.

[17] C. Karpuz, A. K. Gorur, and M. Emur, "Quad-band microstrip bandstop filter design using dual-mode open loop resonators having thin film capacitors," *IEEE Microwave and Wireless Components Letters*, vol. 26, no. 11, pp. 873–875, 2016.

[18] J. Ai, Y. Zhang, K. Xu, M. Shen, T. Ma, and W. T. Joines, "Miniaturized quad-band bandstop filter with controllable frequencies using multiple-mode resonator," in *Proceedings of the2017 IEEE International Symposium on Antennas and Propagation & USNC/URSI National Radio Science Meeting*, pp. 2267-2268, IEEE, San Diego, CA, USA, July 2017.

[19] J. Xu, Z.-Y. Chen, and Q.-H. Cai, "Design of miniaturized dual-band low-pass-bandpass and bandpass filters," *IEEE Transactions on Components, Packaging, and Manufacturing Technology*, vol. 8, no. 1, pp. 132–139, 2018.

[20] D. K. Choudhary and R. K. Chaudhary, "Compact lowpass and dual-band bandpass filter with controllable transmission zero/center frequencies/passband bandwidth," *IEEE Transactions on Circuits and Systems II: Express Briefs*, vol. 67, no. 6, pp. 1044–1048, 2020.

[21] K. Fertas, F. Ghanem, M. Challal, and R. Aksas, "Design and development of compact reconfigurable tri-stopband bandstop filter using hexagonal metamaterial cells for wireless applications," *Progress In Electromagnetics Research M*, vol. 80, pp. 93–102, 2019.

[22] J. Hao, A. Djouadi, F. Rault, X. Tao, É. Lheurette, and L. Burgnies, "Multiresonant split ring resonator with meandered strips," *Physica Status Solidi (A) Applications and Materials Science*, vol. 217, pp. 1–5, 2020.

[23] A. B. Numan and M. S. Sharawi, "Extraction of material parameters for metamaterials using a full-wave simulator [education column]," *IEEE Antennas and Propagation Magazine*, vol. 55, no. 5, pp. 202–211, 2013.

[24] A. N. Plastikov, "About two approaches to automation of a process of calculating metamaterial parameters according to the scattering-parameter extraction method using modern full-wave simulators," in *Proceedings of the 2017 Progress In Electromagnetics Research Symposium - Spring (PIERS)*, pp. 3763–3767, Saint Petersburg Russia, May 2017.

[25] D. R. Smith, D. C. Vier, T. Koschny, and C. M. Soukoulis, "Electromagnetic parameter retrieval from inhomogeneous metamaterials," *Physical review. E, Statistical, nonlinear, and soft matter physics*, vol. 71, pp. 036617–36711, 2005.

[26] J.-M. Yan, L. Cao, and H.-Y. Zhou, "A novel quad-band bandstop filter based on coupled-line and shorted stub-loaded half-wavelength microstrip resonator," *Progress in Electromagnetics Research Letters*, vol. 79, pp. 65–70, 2018.

[27] X. Min and H. Zhang, "Compact triple-band bandstop filter using folded, symmetric stepped-impedance resonators," *AEU - International Journal of Electronics and Communications*, vol. 77, pp. 105–111, 2017.

[28] M. Faisal, S. Khalid, M. U. Rehman, and M. A. Rehman, "Synthesis and design of highly selective multi-mode dual-band bandstop filter," *IEEE Access*, vol. 9, pp. 43316–43323, 2021.

[29] A. Rajput, M. Chauhan, and B. Mukherjee, "A novel multi wideband bandstop filter with annular shaped stubs," *AEU - International Journal of Electronics and Communications*, vol. 142, Article ID 153993, 2021.

[30] A. Kamma and J. Mukherjee, "Multiple band notch and Dual-Band filter using concentric and contiguous split ring resonators (CCSRR)," *Journal of Electromagnetic Waves and Applications*, vol. 31, no. 1, pp. 57–71, 2017.